Adsorbate-Localized versus Substrate-Mediated Excitation Mechanisms for Generation of Coherent Cs–Cu Stretching Vibration at Cu(111)

ARTICLE *in* THE JOURNAL OF PHYSICAL CHEMISTRY A · MAY 2011

Impact Factor: 2.69 · DOI: 10.1021/jp112307k · Source: PubMed

4 AUTHORS, INCLUDING:

Yoshi Matsumoto
Kyoto University
136 PUBLICATIONS **1,748** CITATIONS
SEE PROFILE

Tomokazu Yasuike
The Open University of Japan
25 PUBLICATIONS **369** CITATIONS
SEE PROFILE

THE JOURNAL OF PHYSICAL CHEMISTRY A

ARTICLE

pubs.acs.org/JPCA

Adsorbate-Localized versus Substrate-Mediated Excitation Mechanisms for Generation of Coherent Cs−Cu Stretching Vibration at Cu(111)

Kazuya Watanabe,[†,§] Yoshiyasu Matsumoto,[*,†] Tomokazu Yasuike,[‡] and Katsuyuki Nobusada[*,‡]

[†]Department of Chemistry, Graduate School of Science, Kyoto University, Kyoto 606-8502, Japan

[‡]Institute for Molecular Science and The Graduate University for Advanced Studies (SOKENDAI), Myodaiji, Okazaki, Aichi 444-8585, Japan

ABSTRACT: Coherent Cs−Cu stretching vibration at a Cu(111) surface covered with a full monolayer of Cs is observed by using time-resolved second harmonic generation spectroscopy, and its generation mechanisms and dynamics are simulated theoretically. While the irradiation with ultrafast pulses at both 400 and 800 nm generate the coherent Cs−Cu stretching vibration at a frequency of 1.8 THz (60 cm^{-1}), they lead to two distinctively different features: the initial phase and the pump fluence dependence of the initial amplitude of coherent oscillation. At 400 nm excitation, the coherent oscillation is nearly cosine-like with respect to the pump pulse and the initial amplitude increases linearly with pump fluence. In contrast, at 800 nm excitation, the coherent oscillation is sine-like and the amplitude is saturated at high fluence. These features are successfully simulated by assuming that the coherent vibration is generated by two different electronic transitions: substrate d-band excitation at 400 nm and the quasi-resonant excitation between adsorbate-localized bands at 800 nm, i.e., possibly from an alkali-induced quantum well state to an unoccupied state originating in Cs 5d bands or the third image potential state.

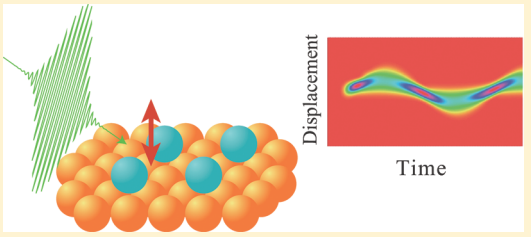

1. INTRODUCTION

Chemisorption of atoms and molecules on metal surfaces frequently introduces adsorbate-induced electronic bands at near the Fermi level. Thermal excitation and de-excitation of electron−hole pairs occurring at near metal surfaces couple to adsorbate nuclear motions via charge transfer between bulk and the adsorbate-induced bands. This type of nonadiabatic coupling between electrons and adsorbate nuclei is ubiquitous at metal surfaces. Thus, the nonadiabatic coupling is a central issue for an understanding of adsorbate dynamics such as vibrational relaxation, diffusion, desorption, and reaction at metal surfaces.[1−8]

The irradiation with ultrafast laser pulses to metal surfaces opens a way to investigate the nonadiabatic coupling and its effects on adsorbate dynamics.[9,10] If electronic excitation by photon absorption causes modulations in the electron density relevant to bonds of adsorbate or bonds between adsorbate and substrate, vibrational modes associated with the bonds are stimulated. When the time scale of modulations induced by light pulses is much shorter than the period of a vibration of interest, this vibration mode can be excited coherently: the generation of coherent surface phonons.

The equation of motion of the amplitude Q of the relevant coherent vibrational mode can be described as a forced harmonic oscillator with damping

$$\frac{d^2Q}{dt^2} + 2\beta\frac{dQ}{dt} + \Omega_0{}^2Q = \frac{F(t)}{\mu} \quad (1)$$

Here, $\Omega_0/2\pi$ is the natural frequency of the undamped oscillator, β is the damping rate, μ is the effective mass of the oscillator, and $F(t)$ is the force to generate the coherent motion. With this driving force, the system shows decaying oscillation with the damping rate β

$$Q(t) \propto \cos(\Omega_1 t - \phi)e^{-\beta t} \quad (2)$$

where $\Omega_1 = (\Omega_0{}^2 - \beta^2)^{1/2}$ and ϕ is the initial phase. In general, the initial phase is described as[11]

$$\tan\phi = \frac{\mathrm{Im}[i\tilde{F}(-\Omega_1 - i\beta)]}{\mathrm{Re}[i\tilde{F}(-\Omega_1 - i\beta)]} \quad (3)$$

Here, $\tilde{F}(\Omega)$ is the Fourier transform of $F(t)$. If the force is impulsive, i.e., $F(t) \propto \delta(t)$, the initial phase is $\pi/2$: the nuclear oscillation is described as $Q(t) \propto \exp(-\beta t)\sin\Omega_1 t$. If the force has a temporal profile of a step function, $F(t) \propto \theta(t)$, the initial phase is 0 or π. Therefore, the initial phase provides useful information of the temporal profile of F.

Two major mechanisms have been proposed for bulk coherent phonon excitation: impulsive stimulated Raman scattering (ISRS) and displacive excitation of coherent phonons

Special Issue: David W. Pratt Festschrift

Received: December 28, 2010
Revised: April 12, 2011
Published: May 03, 2011

(DECP).[12] In the ISRS mechanism, phonon modes are excited coherently as a result of mixing between the frequency components ω_i and ω_j that satisfy the vibrational resonant condition, $\omega_i - \omega_j = \Omega_1$, via stimulated Raman scattering. In the DECP mechanism, the equilibrium positions of ions are suddenly displaced by a real electronic transition that promotes either electrons in an empty band or holes in an occupied band; thus the ions start to oscillate around new equilibrium positions. Merlin and co-workers developed the transient stimulated Raman scattering model, including both ISRS and DECP mechanisms on an equal footing.[13,14] If the lifetime of the excited state is substantially longer than the relaxation time of coherent phonons, the system falls into the DECP limit. Riffe and Sabbah[11] modified the model to include the effect of a finite excited state lifetime. Thus, the refined model can treat the case where the excited state lifetime is very short; the force exerted on nuclei can be impulsive even in the DECP mechanism.

One of the most important issues in the study of coherent phonons at metal surfaces is to determine what electronic transition is most responsible for the creation of them. Irradiation with photons at adsorbate on metal surfaces leads to various electronic transitions. However, not all of them are effective to initiate adsorbate nuclear motions. Obviously coherent phonons are effectively generated if photons excite the adsorbate-localized states that are responsible for bonding to the surface. Thus, it is necessary to sort out electronic transitions regarding this point. Two extreme cases have been frequently discussed in the studies of photoinduced surface processes: adsorbate-localized excitation versus substrate-mediated excitation.[15] In the former case a direct transition between adsorbate-localized states initiates adsorbate nuclear motions. In the latter case, hot electrons or holes near the surface created by excitation of bulk states are resonantly scattered and transiently trapped in the adsorbate-localized states, leading to nuclear motions.[16]

We have conducted a systematic study on coherent surface phonons of alkali overlayers on metal surfaces and their decay characteristics using time-resolved second harmonic generation (TRSHG).[10,17] Upon femtosecond laser irradiation of metal surfaces covered with a nearly full monolayer of alkali-metal atoms, alkali−substrate stretching modes are excited coherently. For the adsorption systems of Na[18] and K on Cu(111),[19] the initial amplitudes of alkali−Cu stretching modes are proportional to absorbance of bulk copper. This indicates that substrate excitation plays a major role in generating the coherent phonons at the alkali overlayers. In contrast, at low coverages, Petek and co-workers reported that "frustrated" desorption of Cs is induced by excitation between surface localized states: from the surface state of Cu(111) to the Cs−Cu antibonding state.[20,21] However, there have been no clear observations indicating that adsorbate-localized excitation generates coherent phonons at alkali-covered metal surfaces at nearly full monolayer coverages.

The Cs monolayer on Cu(111) provides a good opportunity to elucidate the excitation mechanisms of surface coherent phonons. At high coverages, the alkali monolayer constructs two occupied metallic surface bands: an overlayer resonance (OR) located below the L-band gap of Cu(111) and a quantum well state (QWS) at around the Fermi level.[17,22−24] Because QWS is located in the L-band gap, its wave function is localized at the surface. In addition, an unoccupied band originating from the Cs 5d band is located at ∼1.6 eV above the Fermi level.[25] Thus, the resonance transition from QWS to the unoccupied Cs 5d band is expected to take place at around 1.6 eV. Note that no transitions take place from bulk Cu d bands at $h\nu$ = 1.6 eV, because the top of the Cu d bands are located at ∼2.0 eV below the Fermi level. Consequently, it is possible to examine how the characteristics of surface coherent phonons depend on the nature of electronic excitation: adsorbate-localized excitation versus substrate-mediated excitation.

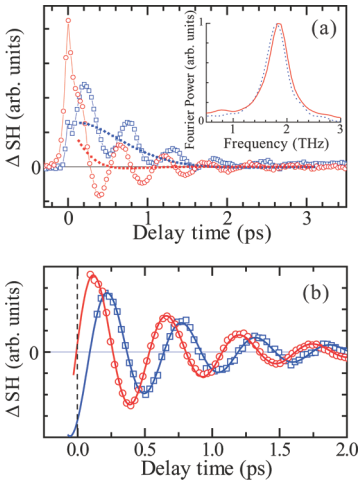

Figure 1. (a) Excitation wavelength dependence of TRSHG traces taken from Cs/Cu(111) at λ_{ex} = 800 nm (red open circles) and λ_{ex} = 400 nm (blue open squares). The probe wavelength is 565 nm for both traces. The incident pump fluence was 8.0 mJ/cm^2 and the Cs coverage was 0.23 ML at λ_{ex} = 800 nm; 3.6 mJ/cm^2 and 0.25 ML at λ_{ex} = 400 nm. Solid lines are results of the nonlinear least-squares fitting with eq 4. Dotted lines are overdamped components contributed by hot electrons. Inset: Fourier power spectra of the oscillatory components of the TRSHG traces for λ_{ex} = 800 nm (solid) and for λ_{ex} = 400 nm (dotted). (b) Oscillating components obtained by subtracting the overdamped ones. Note that initial phases are very different, while the frequencies are very similar.

This paper describes that coherent Cs−Cu stretching vibration is excited by not only substrate excitation but also adsorbate-localized excitation. First, we show that the initial phase of coherent Cs−Cu stretching and the pump fluence dependence of the initial amplitude are very different between the photon energies of pump pulses at $h\nu$ > 2.2 and 1.55 eV. Then we describe theoretical treatment that simulates these behaviors in terms of adsorbate-localized and substrate-mediated excitations.

2. TRSHG MEASUREMENTS

2.1. Experimental Method. The experiments were carried out in an ultrahigh vacuum chamber equipped with a cylindrical analyzer for Auger electron spectroscopy (AES) and low energy electron diffraction (LEED). Cs atoms from a degassed alkali dispenser (SAES Getters) were deposited on a clean Cu(111) surface at 90−110 K. Cs coverage θ was monitored by measuring the ratio r of AES intensity at 557 eV (Cs:LMM) to that at 917 eV (Cu:LMM) as a function of Cs deposition time. According to the literature,[26,27] the Cs saturation coverage is 0.28 ML (1 ML corresponds to the atomic density of a clean Cu(111) surface, 1.8 × 10^{15} cm^{-2}). The deposition time to saturate the first layer of Cs was determined by observing a sudden change in the slope of r with respect to deposition time. Coverages other than 0.28 ML were determined from deposition time under the assumption

dx.doi.org/10.1021/jp112307k |J. Phys. Chem. A 2011, 115, 9528–9535

Table 1. Parameters Obtained by Fitting TRSHG Traces in Figure 1 to Equation 4[a]

λ_{ex} (nm)	a_i	ν_i (THz)	τ_i (ps)	ϕ_i (deg)
800	0.53	1.84 ± 0.01	0.73 ± 0.02	−84 ± 1
	0.47	0.48 ± 0.13	0.25 ± 0.02	−4 ± 24
400	0.34	1.82 ± 0.01	0.78 ± 0.02	−149 ± 1
	0.66	0.23 ± 0.01	0.53 ± 0.04	−64 ± 5

[a] The amplitude a_i is normalized to satisfy $\Sigma_i|a_i| = 1$ for each trace.

of a constant deposition rate. At $\theta = 0.25$ ML, the appearance of a (2×2) LEED pattern was confirmed.

TRSHG measurements were performed in a similar way to that reported previously.[19] The output of a Ti:sapphire regenerative amplifier (800 nm, pulse duration = 130 fs, and repetition rate = 1 kHz) was split into two. One half of the output was used for pumping a home-built noncollinear optical parametric amplifier (NOPA). The NOPA system supplied 25 fs pulses with a center wavelength at 565 nm: these pulses were used as either pump or probe pulses. The other half (800 nm) was compressed by focusing into a cylindrical tube filled with Kr gas (ca. 2 atm) and by using subsequent multiple reflections on negative group velocity dispersion mirrors. The compressed pulse width was estimated to be ~50 fs. We used the compressed 800 nm pulse as a pump and the output of the NOPA (565 nm) as a probe. We also used a 400 nm pulse as a pump that was obtained by doubling the frequency of compressed 800 nm pulses with a BBO (β-BaB_2O_4) crystal; the pulse width was estimated to be ~60 fs. In the TRSHG measurements, p-polarized pump and probe pulses were focused onto the sample surface at an incident angle of ~70°. An optical chopper modulated the pump beam for phase-sensitive detection of pump-induced changes in SH intensity $\Delta I_{SH}(t) = (I_{SH}(t) - I^0_{SH})/I^0_{SH}$, where $I_{SH}(t)$ and I^0_{SH} are SH intensities at a delay time t with and without pump pulses, respectively.

2.2. Phonon Frequency. Both excitations at the wavelengths $\lambda_{ex} = 400$ and 800 nm generate coherent surface phonons at a Cu(111) surface covered with Cs. Figure 1a shows typical traces of TRSHG signals. The trace measured upon excitation at $\lambda_{ex} = 800$ nm shows a distinct peak at $t = 0$ ps and a subsequent oscillating component lasting over $t \sim 3$ ps, while the trace at $\lambda_{ex} = 400$ nm shows a less pronounced peak at $t = 0$ ps followed by a similar oscillatory component. To analyze the TRSHG traces quantitatively, we fitted the traces in $t \geq 130$ fs to a sum of damped cosinusoides

$$\Delta I_{SH}(t) = \sum_i a_i \exp(-t/\tau_i) \cos(2\pi\nu_i t + \phi_i) \quad (4)$$

where the ith damped oscillatory component is characterized with the relative amplitude a_i, the frequency ν_i, the initial phase ϕ_i, and the dephasing time τ_i. The traces were well fitted by two components: an oscillatory component with $\nu \sim 1.8$ THz and an overdamped low frequency mode with $\nu = 0.2-0.5$ THz. The parameters obtained by the fittings are summarized in Table 1. The inset of Figure 1a shows the Fourier power spectra of the oscillatory components obtained by subtracting the overdamped components. The oscillation frequency and the decay time are almost insensitive to λ_{ex}. The frequency at $\nu = 1.8$ THz is close to that of Cs−Cu stretching observed with helium atom scattering for Cs/Cu(001)[28] and that calculated for Cs/Cu(111).[29] Thus, we attributed this higher frequency component to Cs−Cu stretching. The lower frequency overdamped components are due to electronic response and mainly reflect population dynamics of hot electrons in the bulk Cu. The relative contribution of the overdamped component to TRSHG signals at $0 < t < 1$ ps is larger for $\lambda_{ex} = 400$ nm than that for $\lambda_{ex} = 800$ nm. This is because the absorbance of bulk Cu at 800 nm is only 12% of that at 400 nm at an incident angle of 70°; hot electron density at $\lambda_{ex} = 400$ nm is substantially higher than that at $\lambda_{ex} = 800$ nm.

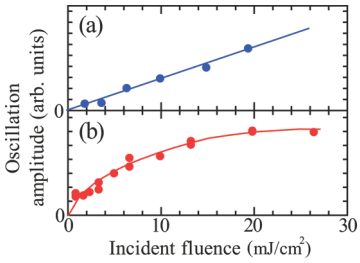

Figure 2. Incident pump fluence dependence of the initial amplitude of oscillation in TRSHG traces for (a) $\lambda_{ex} = 400$ nm (blue) and (b) $\lambda_{ex} = 800$ nm (red). Solid lines are guides to the eye.

2.3. Initial Phase. Although both TRSHG traces at $\lambda_{ex} = 800$ and 400 nm show a prominent oscillating component with $\nu = 1.8$ THz, the initial phase of the oscillating component at $\lambda_{ex} = 800$ nm is very different from that at $\lambda_{ex} = 400$ nm, as shown in Figure 1b. Fitting of TRSHG traces to eq 4 determined the initial phases: $\phi = (-84 \pm 1)°$ at $\lambda_{ex} = 800$ nm and $(-149 \pm 1)°$ at $\lambda_{ex} = 400$ nm. We also examined TRSHG traces at $\lambda_{ex} = 565$ nm obtained by using 800 nm pulses as a probe; this resulted in $\phi = (-147 \pm 2)°$. Thus, Cs−Cu stretching is sine-like at $\lambda_{ex} = 800$ nm, while this is close to cosine-like at $\lambda_{ex} = 400$ and 565 nm.

The initial phase is not sensitive to Cs coverage nor pump fluence. At $\lambda_{ex} = 800$ nm, the initial phase fell in the range from −81° to −103° in the Cs coverage range from $\theta = 0.20$ to 0.26 ML and in the pump fluence range from $I = 8$ to 25 mJ/cm^2. At $\lambda_{ex} = 400$ nm, ϕ fell in the range from −144° to −161° in $\theta = 0.23-0.25$ ML and $I = 3.6-12.6$ mJ/cm^2. Therefore, the tendency, sine-like at $\lambda_{ex} = 800$ nm and close to cosine-like at $\lambda_{ex} = 400$ nm, still holds in those coverage and pump fluence ranges. This clear excitation wavelength dependence of the initial phase indicates that electronic excitation responsible for coherent phonon generation is different between $\lambda_{ex} = 400$ and 800 nm.

2.4. Pump Fluence Dependence of Amplitude. In addition to the initial phase, the pump fluence dependence of the oscillation amplitude is very different between $\lambda_{ex} = 400$ and 800 nm. Initial amplitudes are plotted as a function of averaged incident fluence of pump pulses in Figure 2. While the amplitude at $\lambda_{ex} = 400$ nm increases linearly with the pump fluence, the amplitude at $\lambda_{ex} = 800$ nm saturates at $I \sim 20$ mJ/cm^2. Because the reflectivity of Cu surface is 32% at 400 nm and 92% at 800 nm under the current optical geometry, the energy absorbed by bulk copper at 800 nm is much smaller than that at 400 nm. However, the amplitude at $\lambda_{ex} = 800$ nm deviates from linearity at moderate incident fluence: $I \sim 2$ mJ/cm^2. Thus, it is unlikely that bulk excitation is responsible for generation of coherent phonons at $\lambda_{ex} = 800$ nm.

2.5. Summary of Experimental Results. The frequency of the major oscillating components in TRSHG traces, $\nu = 1.8$ THz, does not depend on the wavelength used in the current work: $\lambda_{ex} = 400$, 565, and 800 nm. This frequency component is attributable to the coherent phonon mode of Cs−Cu stretching.

In contrast, the initial phase and the pump-fluence dependence of amplitude clearly depend on the excitation wavelength. The difference in initial phase indicates that the force exerted on Cs strongly depends on the excitation wavelength: the force is close to impulsive at λ_{ex} = 800 nm, whereas it is close to displacive at λ_{ex} = 565 and 400 nm. Moreover, the difference in the pump-fluence dependence of amplitude indicates that the electronic transitions responsible for generating coherent phonons are different between λ_{ex} = 800 nm and λ_{ex} = 565 and 400 nm.

We have studied the excitation mechanism of alkali−Cu coherent phonons at Cu(111) surfaces adsorbed by Na[18] and K.[19] Both Na−Cu and K−Cu coherent phonons are created when the pump photon energy exceeds 2 eV. The initial phases of oscillating components due to alkali−Cu stretching are −165° for Na and (10 ± 10)° for K; all are cosine-like oscillations. Thus, the coherent phonons of Cs−Cu stretching at λ_{ex} = 565 and 400 nm share similar features to Na and K adsorption systems. We have demonstrated that Na− and K−Cu coherent stretching motions are mediated by substrate excitation, because the action spectra of the oscillation amplitude coincide with the absorbance curve of bulk Cu;[18,19] the strong absorption due to the transition from the d band to the unoccupied states just above the Fermi level starts at around 2.2 eV. Therefore, we can generalize that substrate excitation of d bands generates displacive force to alkali adsorbates on Cu(111). In this context, the appearance of Cs−Cu coherent phonons at λ_{ex} = 800 nm is exceptional. For K adsorption on Cu(111), we did not observe any coherent excitation at λ_{ex} = 800 nm. This adsorbate-specific excitation can be rationalized by excitation between adsorbate-localized states, because their energy levels depend on alkali adsorbates and their coverages. Furthermore, the saturation effect in the pump-fluence dependence at λ_{ex} = 800 nm is characteristic to excitation of localized states. Therefore, the experimental results obtained in this study definitely indicate that electronic transitions responsible for creation of coherent Cs−Cu stretching vibration depend on the excitation wavelength: adsorbate-localized excitation at λ_{ex} = 800 nm and substrate excitation at λ_{ex} < 565 nm.

3. THEORETICAL SIMULATION

3.1. Electronic Structure. The electronic structure of Cs on Cu(111) has been studied experimentally[24,25,30,31] and theoretically.[24,32,33] The electronic structure strongly depends on Cs coverage. At low coverage below 0.1 ML, Cs adsorption induces an unoccupied state at ∼3 eV above the Fermi level. This state is attributed to 6s resonance; the 6s state of a free Cs atom is lifted owing to the Coulomb interaction among the 6s electron, the Cs ionic core, and the induced image charge in the copper substrate.[33]

When alkali coverage increases, the interactions among Cs atoms are significant. First-principles calculations of free-standing alkali layers in vacuum clearly showed that 6s, 6p, and 5d orbitals of Cs form two-dimensional bands.[32,34] This integrity is held when the free-standing alkali layer is brought to the copper surface. They are stabilized by interactions with substrate. The 6s band becomes an overlayer resonance located at around −1.0 eV, whereas the partially occupied 6p band is located at −0.025 eV, which was observed with angle-resolved photoemission;[24] this band is in the Shockley inverted band gap so that the band forms a quantum well state (QWS). The unoccupied Cs 5d band is located at ∼1.6 eV, which was identified with inverse photoemission.[25] Furthermore, according to density functional theory calculations,[32] the third image-potential state (IPS) at $\bar{\Gamma}$ is also located at ∼1.6 eV.

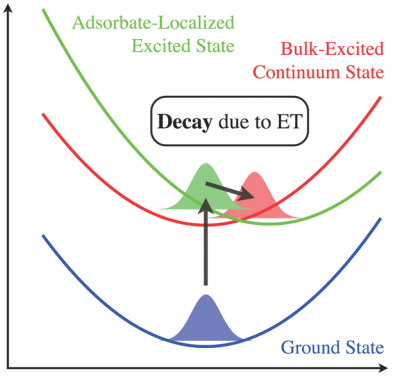

Figure 3. Schematic representation of the potential energy curves (PECs) of the ground state (blue), the adsorbate-localized excited state (green), and the bulk continuum states (red). The transient-adsorbate mediation mechanism is also depicted. In this mechanism, the wave packet is initially created at the displaced adsorbate-localized PEC via a resonant transition, and started to propagate on the PEC. Rapid quenching of the excited state brings the wave packet on the PEC of bulk continuum states, then the wave packet oscillates on the surface.

Because the symmetry allowed transition from QWS to either the Cs 5d band or the third IPS is expected to be resonant at around 1.6 eV, pump pulses at 800 nm (1.55 eV) of a Ti:sapphire laser conveniently allow us to excite this transition resonantly. Although Cu substrate also absorbs photons at this wavelength, absorbance at 800 nm is much smaller than those at λ < 565 nm, because the strong transitions from the occupied d bands of Cu take place at λ < 565 nm. These considerations and the experimental results summarized in the previous section lead us to postulate that excitation at 800 nm is dominated by the resonant transition from QWS to the unoccupied adsorbate-localized state, whereas excitations of bulk Cu d bands contribute to coherent phonon creation at λ < 565 nm. In the following sections, we show that the two different excitation schemes account for the differences in initial phase and fluence dependence observed experimentally.

3.2. Cs−Cu Potential Energy Curves. To simulate photo-induced coherent adsorbate dynamics, one needs potential energy curves (PECs) of both ground and excited electronic states. Here we construct simple model PECs to extract essential features of coherent nuclear dynamics for Cs/Cu(111), instead of calculating them with first-principles methods, because it is rather difficult to calculate the excited state PECs of adsorbate on metal surfaces in particular.

First, the PEC of the ground state is modeled with a harmonic function

$$V_g(Z) = \frac{1}{2} m_{Cs} \omega_g^2 (Z - Z_{eg})^2 \qquad (5)$$

where m_{Cs} is the mass of Cs atom, ω_g is the vibration frequency of Cs−Cu stretching, and Z_{eg} is the equilibrium position of Cs atom. We assume that $\omega_g/2\pi$ = 1.85 THz (7.65 meV) and Z_{eg} = 0.30 nm.[35]

For excited states, we have two classes of PEC to implement adsorbate-localized and substrate-mediated excitations. The adsorbate-localized excited state, originating in the Cs 5d band or the third IPS, has a finite width Γ because of interactions with

dx.doi.org/10.1021/jp112307k | J. Phys. Chem. A 2011, 115, 9528–9535

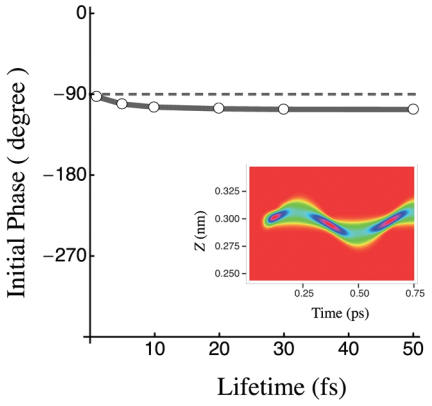

Figure 4. Initial phases calculated from TAM model as a function of the lifetime of the excited state. They deviate slightly from $\phi = -90°$ (dashed line). Inset: the time evolution of the wave packet $\Psi_b{}^{\varepsilon}$ (ε = 1.55 eV, τ = 30 fs).

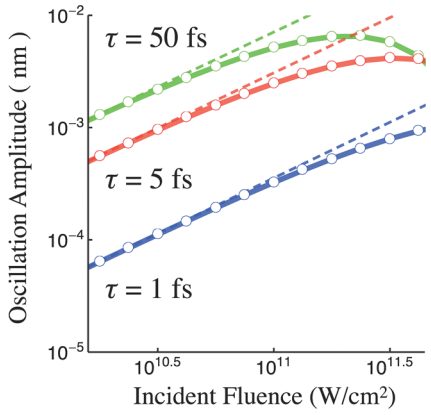

Figure 5. Simulated incident fluence dependences of the amplitude of coherent Cs oscillation induced by excitation between the adsorbate-localized states at $h\nu$ = 1.55 eV. The excited-state lifetime is assumed to be 1 (blue), 5 (red), and 50 fs (green). The amplitudes deviate from linearity (dashed lines) at high fluences.

bulk continuum electronic states. Thus, the eigenenergy of the resonance state is given by a complex value $E = E_r - i\Gamma/2$, where the imaginary part is related to the lifetime $\tau = -\hbar/2Im(E) = \hbar/\Gamma$. In the present work, we modeled the PEC of the adsorbate-localized excited state by the following function

$$V_e(Z) = \frac{1}{2} m_{Cs}\omega_e{}^2(Z - Z_{ee})^2 + \Delta E - i\frac{\Gamma}{2} \qquad (6)$$

where ω_e and Z_{ee} are the vibration frequency and the equilibrium position of the excited state, respectively, and ΔE is the energy offset from the ground state. Here we assume $\omega_e = \omega_g$ and $Z_{ee} = 1.15Z_{eg}$; the assumption of $Z_{ee} \neq Z_{eg}$ is naturally required, because the adsorbate-localized excitation largely changes the interaction between adsorbate and surface. The energy offset ΔE is set to 1.36 eV in such a way that the vertical excitation energy from the equilibrium position of Cs in the ground state is 1.55 eV, corresponding to the experimentally detected adsorbate-localized excitation.[25] The lifetime of the excited state is not available for high Cs coverages employed in our experiments. Here, we assume that the lifetime is in the range from several to several tens of femtoseconds; this is much shorter than the period of Cs−Cu stretching mode (~0.54 ps). Under this assumption a wave packet prepared in the excited state PEC does not propagate in the wide range. Thus, the details of the real part of $V_e(Z)$ are not so important.

Because the bottom of the QWS band is located at very close to the Fermi level, the band is occupied in a limited range of the parallel momentum $K_{\parallel}$ around $\bar{\Gamma}$, resulting in a narrow bandwidth, 40 meV at 170 K.[24] Thus, we neglect any $K_{\parallel}$ dependence of the PEC of the adsorbate-localized excited state.

The bulk excited states are composed of a continuum caused by electron−hole pair creations in bulk bands. Unless bulk excitations lead to electron transfer to the adsorbate-localized unoccupied band, they do not directly trigger Cs nuclear motions. Thus, the potential energy curves of the bulk excited states $V_b{}^{\varepsilon}(Z)$ are reasonably assumed to have the same Z dependence as $V_g(Z)$ but shifted vertically by energy offset ε

$$V_b{}^{\varepsilon}(Z) = V_g(Z) + \varepsilon \qquad (7)$$

where ε corresponds to the excitation energy in the bulk bands.

In summary, our model consists of three types of potential energy curves as shown in Figure 3: the ground and the adsorbate-localized excited states and the continuum states derived from the bulk excitations.

3.3. Adsorbate Dynamics Induced by Adsorbate-Localized Excitation. The adsorbate dynamics induced by the optical excitation to the adsorbate-localized excited state is effectively treated with the three-state coupled scheme as described in the previous paper.[36] The nuclear wave packets of Ψ_g, Ψ_e, and $\Psi_b{}^{\varepsilon}$ on the ground, the adsorbate-localized excited, and the bulk excited continuum states, respectively, propagate according to the following time-dependent Schrödinger equation

$$i\hbar\frac{\partial}{\partial t}\begin{pmatrix}\Psi_e\\ \Psi_b{}^{\varepsilon}\\ \Psi_g\end{pmatrix} = \mathscr{K}\begin{pmatrix}\Psi_e\\ \Psi_b{}^{\varepsilon}\\ \Psi_g\end{pmatrix} \qquad (8)$$

The three-state coupled Hamiltonian $\mathscr{K}$ is given by

$$\mathscr{K} = \begin{pmatrix}\mathscr{T} + V_e(Z) & 0 & -\mu G(t)\\ \sqrt{\frac{\Gamma}{2\pi}} & \mathscr{T} + V_b{}^{\varepsilon}(Z) & 0\\ -\mu G(t) & 0 & \mathscr{T} + V_g(Z)\end{pmatrix} \qquad (9)$$

where $\mathscr{T}$ is the kinetic energy operator, $G(t)$ is the electric field of the applied laser pulse, and μ is the transition dipole moment for the adsorbate-localized excitation, which is assumed to be 1 au. The applied electric field $G(t)$ is given by

$$G(t) = G_0 \exp\left[-\frac{(t - t_{cen})^2}{2\sigma^2}\right] \cos \Omega(t - t_{cen}) \qquad (10)$$

and

$$\sigma = \frac{\text{fwhm}}{2\sqrt{2 \log 2}} \qquad (11)$$

where fwhm is the full-width at half-maximum of the applied Gaussian pulse, $t_{cen} = 2 \times$ fwhm is its time center, G_0 is the peak value of the field, and Ω is the center frequency. The fwhm of the pulse is fixed at 30 fs.

The adsorbate-localized excitation mechanism of adsorbate coherent vibration is schematically depicted in Figure 3, which

dx.doi.org/10.1021/jp112307k |J. Phys. Chem. A 2011, 115, 9528–9535

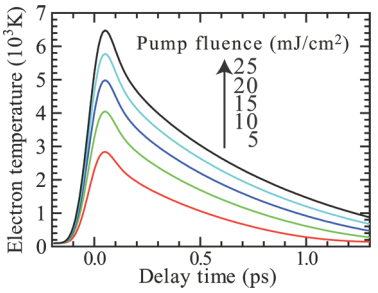

Figure 6. Temporal profiles of electron temperature estimated by the two-temperature model as a function of incident fluence of pump pulses at λ = 400 nm .

has been recently proposed by two of us: the transient-adsorbate mediation (TAM) mechanism.[36] After the irradiation of near-resonant light pulse, the population partially transfers to the adsorbate-localized excited state. The wave packet on this PEC starts to propagate toward vacuum owing to the repulsive force and gains momentum. Because the back-donation of charge to the bulk occurs rapidly, the lifetime of this state is very short. Thus, the quenching of the adsorbate-localized excited state brings the wave packet to the PEC of bulk continuum states, then an oscillatory motion of the wave packet takes place on the PEC, while bulk electrons dissipate energy via electron−phonon coupling.

The time-dependent expectation value of Z for the wave packet on the continuum PECs is calculated as[36]

$$\langle Z_b(t)\rangle = \int_0^\infty \langle \Psi_b{}^{\varepsilon}(t)|Z|\Psi_b{}^{\varepsilon}(t)\rangle \, d\varepsilon \sim \{1-\rho_g(t_\infty)\}\frac{\langle \Psi_b{}^{\hbar\Omega}(t)|Z|\Psi_b{}^{\hbar\Omega}(t)\rangle}{\langle \Psi_b{}^{\hbar\Omega}(t)|\Psi_b{}^{\hbar\Omega}(t)\rangle} \quad (12)$$

where $1-\rho_g(t_\infty)$ corresponds to the energy-integrated population of the continuum states at $t=\infty$. The rapid quenching of the adsorbate-localized excited state results in sine-like oscillation of $\langle Z_b(t)\rangle$ as shown in the inset of Figure 4. The oscillatory profile was fitted to a damped cosinusoide, and the initial phases obtained are plotted in Figure 4 as a function of the excited-state lifetime. Although the initial phase depends on the excited-state lifetime, the deviations from −90° are small. Thus, the adsorbate-localized excitation leads to sine-like oscillation; this is consistent with the experimental observation at λ_{ex} = 800 nm.

Figure 5 shows the incident-fluence dependence of the initial oscillation amplitude. While the oscillation amplitude linearly increases with incident fluence, it deviates from lineality and tends to saturate as fluence becomes high. This is also consistent with the experimental finding at λ_{ex} = 800 nm as shown in Figure 2b. This trend is typical of resonant excitation between localized states: although the population of the adsorbate-localized excited state linearly increases with fluence at low fluence, the transition is saturated at high fluence. The saturation originates primarily in the limited density of states of the initial state: only a small fraction of the QWS band is occupied. While the saturation behavior depends on the transition probability and the excited-state lifetime, it is not possible to determine them independently by simply comparing the experimental results with the simulated ones. Thus, we need to know one of those by other means. The lifetime of a Cs−Cu antibonding state attributed to 6s resonance was reported to be 11−15 fs measured by Aeschlimann and co-workers[37,38] and 15 fs for phase decay and 50 fs for energy decay by Petek and co-workers.[31] It may not

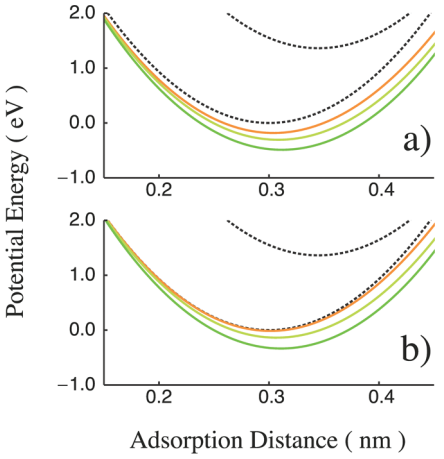

Figure 7. Effective potential energy curves $V_{eff}(Z)$ for quasi-thermal electronic states at the electron temperatures (T_e) of 5000 (orange), 10000 (yellowish green), and 15000 (green) K. The bandwidth of the excited state is (a) 1.0 and (b) 0.1 eV. The dotted curves show $V_g(Z)$ and $V_e(Z)$ at T_e = 0 K.

be appropriate using these values for the excited-state lifetime here, since those two-photon photoemission measurements were performed at low Cs coverages ≤0.1 ML where Cs adatoms are ionic in contrast to metallic in the current experimental condition. However, it is worth estimating some plausible set of transition probability and lifetime. If we assume that a dipole transition moment is 1 au (=2.6 D) with which the oscillation amplitudes in Figure 5 are estimated, the incident fluence dependence curves at τ = 5−50 fs show that the saturation effect becomes appreciable around 3×10^{10} W/cm^2; this is reasonably close to the experimental result, 2 mJ/cm^2 (Figure 2), i.e., a peak power of 4×10^{10} W/cm^2 for the pump pulse.

3.4. Adsorbate Dynamics Induced by Bulk Excitation. Absorption of an intense femtosecond laser pulse generates quasi-thermal equilibrium in the surface electron gas, and its peak temperature reaches several thousand kelvin over a time scale of several hundred femtoseconds.[39,40] Figure 6 shows temporal profiles of electron temperature as a function of incident fluence of pump pulses; those are estimated with the two-temperature model[41,42] by using parameters listed in ref 43. Under the circumstances, the adsorbate-localized state is temporarily occupied with hot electrons. Brandbyge et al.[44] derived the expression of the effective potential energy function $V_{eff}(Z)$ which governs the dynamics of adsorbate

$$V_{eff}(Z) = V_g(Z) - \int_{-\infty}^{\infty} n_F(E,T_e)\delta(E,Z)\,dE \quad (13)$$

where $n_F(E,T_e)$ is the Fermi−Dirac distribution at electron temperature T_e. The function $\delta(E,Z)$ is an effective occupation number of the adsorbate-localized excited state and is defined by the integration of the local density of states for the adsorbate-localized excited state

$$\delta(E,Z) = \frac{1}{\pi}\int_{-\infty}^{E} dE' \frac{\Gamma/2}{(E'-E_r)^2+(\Gamma/2)^2} \quad (14)$$

$$= \frac{1}{2} - \frac{1}{\pi}\arctan\left[\frac{2(E_r-E)}{\Gamma}\right] \quad (15)$$

where $E_r \equiv \mathrm{Re}[V_e(Z)]$ and Γ is the effective bandwidth. If the lifetime of the excited state is very short, the quenching rate

dx.doi.org/10.1021/jp112307k |J. Phys. Chem. A 2011, 115, 9528–9535

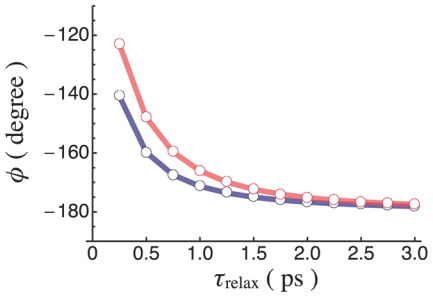

Figure 8. Initial phase plotted against the relaxation time of substrate electrons. The bandwidth of the excited state is assumed to be 1.0 (blue) and 0.1 eV (red). Because of finite relaxation times of substrate electrons, the initial phases deviate from the DECP limit, $\phi = -180°$.

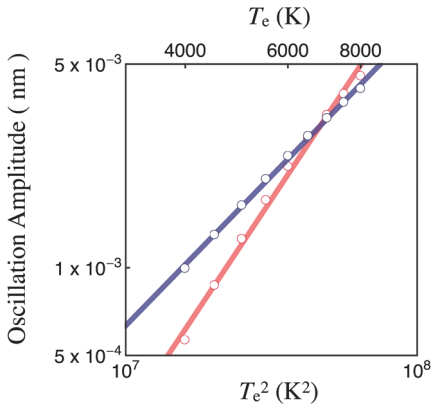

Figure 9. Squared-temperature dependences of the amplitude of coherent Cs oscillation induced by the bulk excitation. The band widths are assumed to be 1.0 (blue) and 0.1 eV (red).

determines the bandwidth: lifetime broadening. Otherwise the dispersion of the band determines the bandwidth. Although the change from $V_g(Z)$ to $V_{eff}(Z)$ was neglected in their original work,[44] we propose that the ultrafast change in the potential energy function induces the coherent adsorbate motion.

Figure 7 shows the effective potential energy curves $V_{eff}(Z)$ for quasi-thermal electronic states generated by bulk excitation. Figure 7a shows the electron-temperature dependence of the potential energy curves for Γ = 1.0 eV. With increasing T_e, $V_{eff}(Z)$ deviates from $V_g(Z)$ more extensively. The changes in the potential energy function are intuitively understood; the partial occupation of the adsorbate-localized excited state makes the position of the potential minimum closer to Z_{ee}. More strictly speaking, the results are interpreted as follows. As shown in eq 13, the changes in the potential energy function are determined by the energy integration of $n_F(E,T_e)\delta(E,Z)$. At a fixed Γ, the integrated value increases with T_e, because the high energy component of $n_F(E,T_e)$ becomes larger at higher T_e. Although this behavior is commonly observed for a narrower band, Γ = 0.1 eV, as shown in Figure 7b, the deviations from $V_g(Z)$ are smaller than those for the band with Γ = 1.0 eV. This is because the smaller Γ gives smaller overlap of $\delta(E,Z)$ with $n_F(E,T_e)$.

Because electron transfer between bulk continuum states and the adsorbate-localized state is expected to occur rapidly, $V_{eff}(Z)$ changes in a sufficiently shorter time scale than that of the Cs motion. This rapid change in $V_{eff}(Z)$ generates a coherent oscillation of Cs adsorbates. The initial phase of the coherent vibration is $-180°$ if the temporal profile of $V_{eff}(Z)$ is a step function: the DECP limit. However, because the electron temperature relaxes, the force exerted on Cs has a finite duration. If the relaxation time of electron temperature is comparable to the period of Cs vibration, the initial phase significantly deviates from $-180°$. Figure 8 shows how the initial phase depends on the relaxation time of hot electrons. For example, the relaxation time of T_e at a fluence of 5 mJ/cm^2 was estimated by fitting the time profile of T_e (Figure 6) to an exponentially decaying function up to $t \leq 1.2$ ps, resulting in τ_{relax} = 560 fs. According to the calculations shown in Figure 8, the initial phase could be in the range between $-145°$ (for Γ = 0.1 eV) and $-160°$ (for Γ = 1 eV); this is in reasonable agreement with the experimental results at λ_{ex} = 400 and 565 nm.

The initial oscillation amplitude can be calculated from the difference between the minimum positions of $V_g(Z)$ and $V_{eff}(Z)$ at t = 0 ps. Because the square of maximum T_e is proportional to the incident fluence,[45] the plot of the initial amplitude versus T_e^2 in Figure 9 shows the fluence dependence of the initial amplitude: the amplitude increases as $I^{1.03}$ for Γ = 1 eV and $I^{1.51}$ for Γ = 0.1 eV. Thus, the fluence dependence for Γ = 1.0 eV is in good agreement with that at λ_{ex} = 400 nm.

4. CONCLUSION

We showed that a coherent Cs−Cu stretching vibration is generated at Cs/Cu(111) by two different electronic excitations: the adsorbate-localized and substrate-mediated excitations. At λ_{ex} = 800 nm (1.55 eV), the observed oscillatory signals due to the coherent vibration is sine-like, and the amplitude is saturated at high pump fluence. Because the photon energy matches the energy difference between QWS and the unoccupied surface band originating in either the 5d band of Cs or the third IPS, we attributed the generation of coherent phonons to the adsorbate-localized transition between the two surface bands. Theoretical simulations suggest that the sine-like oscillation is due to a short lifetime of the excited state. Upon the excitation to the excited state PEC, the wave packet starts to evolve but rapidly quenched to the PEC that has a potential energy landscape essentially same as the ground state. As a result of the rapid sequence of excitation and de-excitation, Cs−Cu stretching starts at the equilibrium position in the ground state PEC, resulting in sine-like oscillation. Because the electronic transition responsible for the generation of coherent motions takes place between the adsorbate-localized bands, the limited density of states of the bands causes the saturation of the transition as the pump fluence increases.

At λ_{ex} = 565 and 400 nm, bulk excitations from the d bands of copper generate the coherent Cs−Cu stretching vibration. In contrast to λ_{ex} = 800 nm, the coherent oscillation is nearly cosine-like and the amplitude of oscillatory signals linearly increases with pump fluence. The force exerted on Cs is generated by transient occupation of the unoccupied adsorbate-localized band by resonant electron transfer from bulk bands: substrate-mediated excitation. Because the excitation takes place much faster than the period of Cs−Cu stretching, the indirect excitation can coherently excite this mode. In the DECP limit, the oscillation should be pure cosine, because Cs atoms oscillate on the displaced potential energy surface. However, we found that the oscillation deviates from the pure cosine function. Theoretical simulations successfully reproduced the deviations of initial phase from pure cosine by considering relaxation of hot electrons. In addition, the simulations verified the linear dependence

of the initial amplitude on the pump fluence if the bandwidth of the unoccupied state is 1.0 eV.

AUTHOR INFORMATION

Corresponding Author

*E-mail: matsumoto@kuchem.kyoto-u.ac.jp; nobusada@ims.ac.jp.

Present Addresses

[§]PRESTO, JST, 4-1-8 Honcho Kawaguchi, Saitama, Japan.

ACKNOWLEDGMENT

This study is supported in part by a Grant-in-Aid for Scientific Research on Priority Area (461 Molecular Theory for Real Systems) from the Ministry of Education, Culture, Sports, Science and Technology (MEXT) of Japan. K.W. gratefully acknowledges financial support by the PRESTO program of JST. We thank Ken-ichi Inoue for his help with measurements.

REFERENCES

(1) Gadzuk, J. W. In *Dynamics*; Hasselbrink, E., Lundqvist, B., Eds.; *Handbook of Surface Science*; Elsevier: Amsterdam, 2008; Vol. 3; Chapter 1, pp 1−28.

(2) Lundqvist, B.; Hellman, A.; Zoric´, I. In *Dynamics*; Hasselbrink, E., Lundqvist, B., Eds.; *Handbook of Surface Science*; Elsevier: Amsterdam, 2008; Vol. 3; Chapter 10, pp 429−524.

(3) Wodtke, A. M.; Tully, J. C.; Auerbach, D. J. *Int. Rev. Phys. Chem.* **2004**, *23*, 513.

(4) Hasselbrink, E. *Surf. Sci.* **2009**, *603*, 1564.

(5) Langreth, D. C.; Persson, M. In *Laser Spectroscopy and Photochmistry on Metal Surfaces*; Dai, H.-L., Ho, W., Eds.; *Advanced Series in Physical Chemistry*; World Scientific: Singapore, 1995; Vol. 5; Chapter 13, pp 498−541.

(6) Persson, B. N. J.; Persson, M. *Solid State Commun.* **1980**, *36*, 175.

(7) Persson, M.; Hellsing, B. *Phys. Rev. Lett.* **1982**, *49*, 662.

(8) Hellsing, B.; Persson, M. *Phys. Scr.* **1984**, *29*, 360.

(9) Frischkorn, C.; Wolf, M. *Chem. Rev.* **2006**, *106*, 4207.

(10) Matsumoto, Y.; Watanabe, K. *Chem. Rev.* **2006**, *106*, 4234.

(11) Riffe, D. M.; Sabbah, A. J. *Phys. Rev. B* **2007**, *76*, 085207.

(12) Zeiger, H. J.; Vidal, J.; Cheng, T. K.; Ippen, E. P.; Dresselhaus, G.; Dresselhaus, M. S. *Phys. Rev. B* **1992**, *45*, 768.

(13) Garrett, G. A.; Albrecht, T.; Whitaker, J. F.; Merlin, R. *Phys. Rev. Lett.* **1996**, *77*, 3661.

(14) Stevens, T. E.; Kuhl, J.; Merlin, R. *Phys. Rev. B* **2002**, *65*, 144304.

(15) Ho, W. In *Laser Spectroscopy and Photochemistry on Metal Surfaces*; Dai, H. L., Ho, W., Eds.; Advanced Series in Physical Chemistry; World Scientific: Singapore, 1995; Vol. 5; Chapter 24, pp 1047−1140.

(16) Hellsing, B.; Chakarov, D. V.; Österlund, L.; Zhdanov, V. P.; Kasemo, B. *J. Chem. Phys.* **1997**, *106*, 982.

(17) Matsumoto, Y.; Watanabe, K. In *Dyanamics at Solid State Surfaces and Interfaces*; Bovensiepen, U., Petek, H., Wolf, M., Eds.; Wiley-VCH Verlag GmbH: Weinheim, Germany, 2010; Vol. 1: Current Developments; Chapter 11, pp 239−262.

(18) Fuyuki, M.; Watanabe, K.; Ino, D.; Petek, H.; Matsumoto, Y. *Phys. Rev. B* **2007**, *76*, 115427.

(19) Watanabe, K.; Inoue, K.-I.; Nakai, I. F.; Fuyuki, M.; Matsumoto, Y. *Phys. Rev. B* **2009**, *80*, 075404.

(20) Petek, H.; Weida, M. J.; Nagano, H.; Ogawa, S. *Science* **2000**, *288*, 1402.

(21) Petek, H.; Nagano, H.; Weida, M. J.; Ogawa, S. *J. Phys. Chem. B* **2001**, *105*, 6767.

(22) Bonzel, H. P. In *Physics and Chemistry of Alkali Metal Adsorption*; Bradshaw, A. M., Ertl, G., Eds.; Elsevier: Amsterdam, 1989.

(23) Gauyacq, J. P.; Borisov, A. G.; Bauer, M *Prog. Surf. Sci.* **2007**, *82*, 244.

(24) Breitholtz, M.; Chis, V.; Hellsing, B.; Lindgren, S.-Å.; Walldén, L. *Phys. Rev. B* **2007**, *75*, 155403.

(25) Arena, D. A.; Curti, F. G.; Bartynski, R. A. *Phys. Rev. B* **1997**, *56*, 15404.

(26) Fan, W. C.; Ignatiev, A. *Phys. Rev. B* **1988**, *37*, 5274.

(27) von Hofe, T.; Kröger, J.; Berndt, R. *Phys. Rev. B* **2006**, *73*, 245434.

(28) Witte, G.; Toennies, J. P. *Phys. Rev. B* **2000**, *62*, R7771.

(29) Nojima, A.; Yamashita, K.; Hellsing, B. *Phys. Rev. B* **2008**, *78*, 035417.

(30) Lindgren, S.-Å.; Walldén, L. *Solid State Commun.* **1978**, *25*, 13.

(31) Ogawa, S.; Nagano, H.; Petek, H. *Phys. Rev. Lett.* **1999**, *82*, 1931.

(32) Chis, V.; Caravati, S.; Butti, G.; Trioni, M. I.; Cabrera-Sanfelix, P.; Arnau, A.; Hellsing, B. *Phys. Rev. B* **2007**, *76*, 153404.

(33) Zhao, J.; Pontius, N.; Winkelmann, A.; Sametoglu, V.; Kubo, A.; Borisov, A. G.; Sanchez-Portal, D.; Silkin, V. M.; Chulkov, E. V.; Echenique, P. M.; Petek, H. *Phys. Rev. B* **2008**, *78*, 085419.

(34) Wimmer, E. *J. Phys. F: Met. Phys.* **1983**, *13*, 2313.

(35) Lindgren, S.-Å.; Walldén, L.; Rundgren, J.; Westrin, P.; Neve, J. *Phys. Rev. B* **1983**, *28*, 6707.

(36) Yasuike, T.; Nobusada, K. *Phys. Rev. B* **2009**, *80*, 035430.

(37) Bauer, M.; Pawlik, S.; Aeschlimann, M. *Phys. Rev. B* **1997**, *55*, 10040.

(38) Bauer, M.; Pawlik, S.; Aeschlimann, M. *Phys. Rev. B* **1999**, *60*, 5016.

(39) Prybyla, J. A.; Heinz, T. F.; Misewich, J. A.; Loy, M. T.; Glownia, J. H. *Phys. Rev. Lett.* **1990**, *64*, 1537.

(40) Misewich, J. A.; Kalamarides, A.; Heinz, T. F.; Höfer, U.; Loy, M. M. *J. Chem. Phys.* **1994**, *100*, 736.

(41) Anisimov, S. I.; Kapeliovich, B. L.; Perel'man, T. L. *Sov. Phys. JETP* **1974**, *39*, 375.

(42) Kaganov, M. I.; Lifshitz, I. M.; Tanatarov, L. V. *Sov. Phys. JETP* **1957**, *31*, 232.

(43) Germer, T. A.; Stephenson, J. C.; Heilweil, E. J.; Cavanagh, R. R. *J. Chem. Phys.* **1994**, *101*, 1704.

(44) Brandbyge, M.; Hedegard, P.; Heinz, T. F.; Misewich, J. A.; Newns, M. D. *Phys. Rev. B* **1995**, *52*, 6042.

(45) Hohlfeld, J.; Wellershoff, S. S.; Güdde, J.; Conrad, U.; Jähnke, V.; Matthias, E. *Chem. Phys.* **2000**, *251*, 237.